ELSEVIER

Computer Methods and Programs in Biomedicine 58 (1999) 133–145

Computer Methods and Programs in Biomedicine

An object-oriented Monte Carlo simulator for 3D cylindrical positron tomographs

H. Zaidi [a,*], A. Herrmann Scheurer [1,b], C. Morel [a]

[a] *Division of Nuclear Medicine, Geneva University Hospital, CH-1211 Geneva 4, Switzerland*
[b] *Institute of Nuclear Physics, University of Lausanne, CH-1015 Lausanne, Switzerland*

Received 29 December 1997; received in revised form 12 June 1998; accepted 30 June 1998

Abstract

Monte Carlo simulation is a very powerful tool in understanding performances of positron tomographs as well as in assessing image reconstruction algorithms and their implementations. We present an object-oriented Monte Carlo simulator developed for 3D positron tomography. Results from phantom simulation studies including absorption and scattering of the photons in the field-of-view are presented. Scatter fractions determined from these studies are in good agreement with measured scatter fractions published in the literature. Limitations and future prospects are discussed.

Keywords: Monte Carlo; PET; Scatter simulation; Image reconstruction; Object-oriented programming

1. Introduction

The Monte Carlo method allows to simulate statistical processes following from the stochastic nature of radiation emission and detection. Consequently, it has been widely utilised in medical radiation physics [1] since more than 30 years and was notably used to develop dosimetry [2] and to simulate characteristics of scintillation cameras [3]. Apart from being thoroughly exploited to model detectors for positron emission tomography (PET) [4–8], Monte Carlo simulation of three-dimensional (3D) PET data has proved to be a very powerful tool to estimate performances of 3D positron tomographs [9–16] as well as to assess 3D image reconstruction algorithms and their implementations [17,18]. Since it allows to obtain separate images of unscattered and scattered events, it helped developing and evaluating 3D attenuation and scatter correction techniques [19,20]. Furthermore, providing its design is easily

* Corresponding author. Tel.: +41 22 3727165; fax: +41 22 3727169; e-mail: hzaidi@dmnu-pet5.hcuge.ch

[1] Present address: Centre for Neuro-Mimetic Systems, Microcomputing Laboratory, Swiss Federal Institute of Technology, CH-1015 Ecublens, Lausanne, Switzerland.

0169-2607/99/$ - see front matter
PII S0169-2607(98)00078-9

extensible, it represents an effective tool for exploring different schemes for sampling the 3D X-ray transform [21].

In PET, pairs of 511 keV photons resulting from electron-positron annihilations are detected in coincidence. A positron emission tomograph contains a set of detectors usually arranged in adjacent rings that surround the field-of-view (FOV) in order to image the spatial distribution of a positron emitting radiopharmaceutical administered to the patient (Fig. 1). In two-dimensional (2D) PET, data acquisition was limited to coincidences detected within the same detector or adjacent detector rings. With the information obtained from detectors belonging to the same detector rings, images representing the tracer distribution in the planes of the detector rings (direct planes) are obtained. With the information obtained from detectors belonging to adjacent detector rings, we reconstruct images representing the tracer distribution in the planes between the detector rings (cross planes). Here, a 3D PET scanner consisting of N detector rings gives (2N-1) images representing the tracer distribution in adjacent cross-sections of a patient. Transverse sections of the image volume obtained are then stacked together to allow the spatial distribution of the radiopharmaceutical to be viewed in 3D. In fully 3D PET, data acquisition is no more limited to coincidences detected within each of the detector rings, but oblique lines of response (LORs) formed from coincidences detected between different detector rings are also used to reconstruct the image.

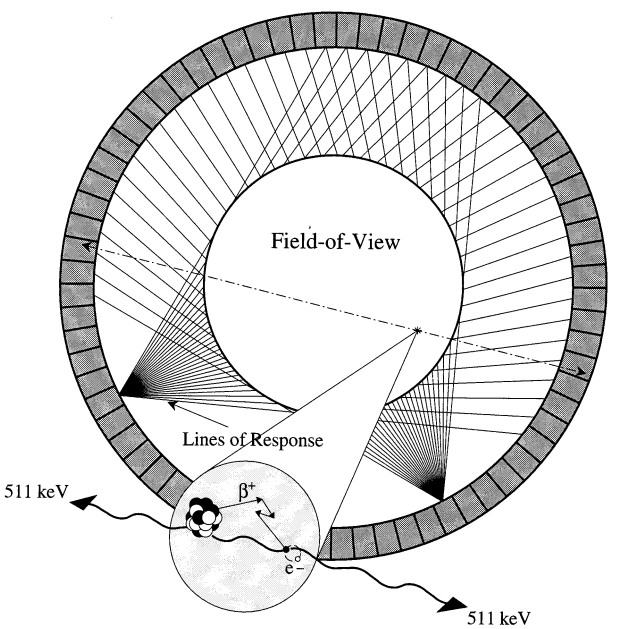

Fig. 1. Originating from the decay of the radionuclide, a positron travels a few mm only to be annihilated by a nearby atomic electron, producing two 511 keV photons emitted in opposite directions. A positron emission tomograph contains a set of detectors usually arranged in adjacent rings surrounding the FOV. Pairs of annihilation photons are detected in coincidence. The size of the FOV is defined by the number of opposite detectors in coincidence.

In addition to true coincidences corresponding to the detection of 511 keV annihilation pairs, scattered and random coincidences are also detected by the imaging system. Fig. 2 illustrates the detection of these different types of coincidences. True coincidences detected for a given LOR allow to estimate the line integral of the annihilation distribution along the LOR, whereas scattered coincidences, where at least one of the two annihilation photons is scattered prior detection, are falsely assigned to the LOR and result in a blurring of the reconstructed image. Random coincidences come from the detection of two non-correlated single photons within the time window set for coincidence measurement and can be easily corrected for.

In this paper, we present an object-oriented Monte Carlo simulator developed for 3D positron tomography. Results from phantom simulation studies including absorption and scattering of the photons in the FOV are presented and future prospects discussed.

2. Methods

2.1. Software description

Unlike procedural programming languages which separate data from operations on data defined by procedures and functions, object-oriented programming languages consist of a collection of interacting high-level units, the objects, that combine both data and operations on data.

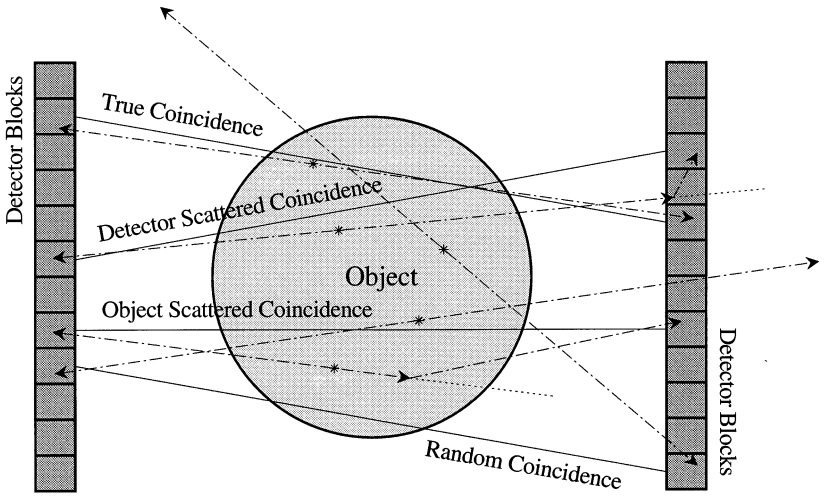

Fig. 2. Schematic of a simulation model for 3D positron tomography. Detection of true, random, object scattered and detector scattered coincidences are indicated along the corresponding LORs. Dash lines indicate photon paths.

This renders objects not much different from ordinary physical objects. This resemblance to real things gives objects much of their power and appeal. They can not only model components of real systems, but equally as well fulfil assigned roles as components in software systems. This programming paradigm appears to be quite well appropriate to Monte Carlo modelling as there is a direct correspondence between objects of the application domain—source and scatter volumes, detectors—and objects of the computational model—source, scatter and detector objects—.

The Monte Carlo simulator, Eidolon, was written in Objective-C [22], an object-oriented programming language based on ANSI C and runs under NextStep 3.3 [23] on an Hewlett-Packard 712/60 workstation with 48 Mb RAM memory. A graphical user interface allows one to select scanner parameters such as the number of detector rings, detector material and sizes, energy discrimination thresholds and detector energy resolution. It also allows one to choose a set of simple 3D shapes, such as parallelepiped, ellipsoid or cylindroid for both the annihilation sources and the scattering media, as well as their respective activity concentrations and chemical compositions. One may view the reference source image and measured 2D coincidence histograms, the sinograms, as they are generated.

2.2. Design and implementation

In order to ease the job of incrementally adding capabilities to the Monte Carlo simulator, a modular design featuring dynamically loadable program elements or bundles was adopted. The basic building block is a model element object class which allows elements to be browsed, inspected, adjusted, created and destroyed through a graphical inspector (Fig. 3). This was then used to implement simple parametric source, detector and scatter object classes and sinogram and image object classes to view and save the generated data. A controller object oversees the simulation process (Fig. 4). The reference image and sinogram displays are periodically updated.

The model assumes a cylindrical array of detector crystals and known spatial distributions of annihilation sources and scatter phantoms. Radial samples are assumed to be equidistant, although ring curvature can be taken into account for sampling. Pairs of annihilation photons are generated uniformly within the source objects, they are tracked until extermination of their history either by interacting with scatter or detector objects, or by escaping the positron tomograph geometry and FOV. Positron range and photon non-collinearity due to thermal motion of the electron-

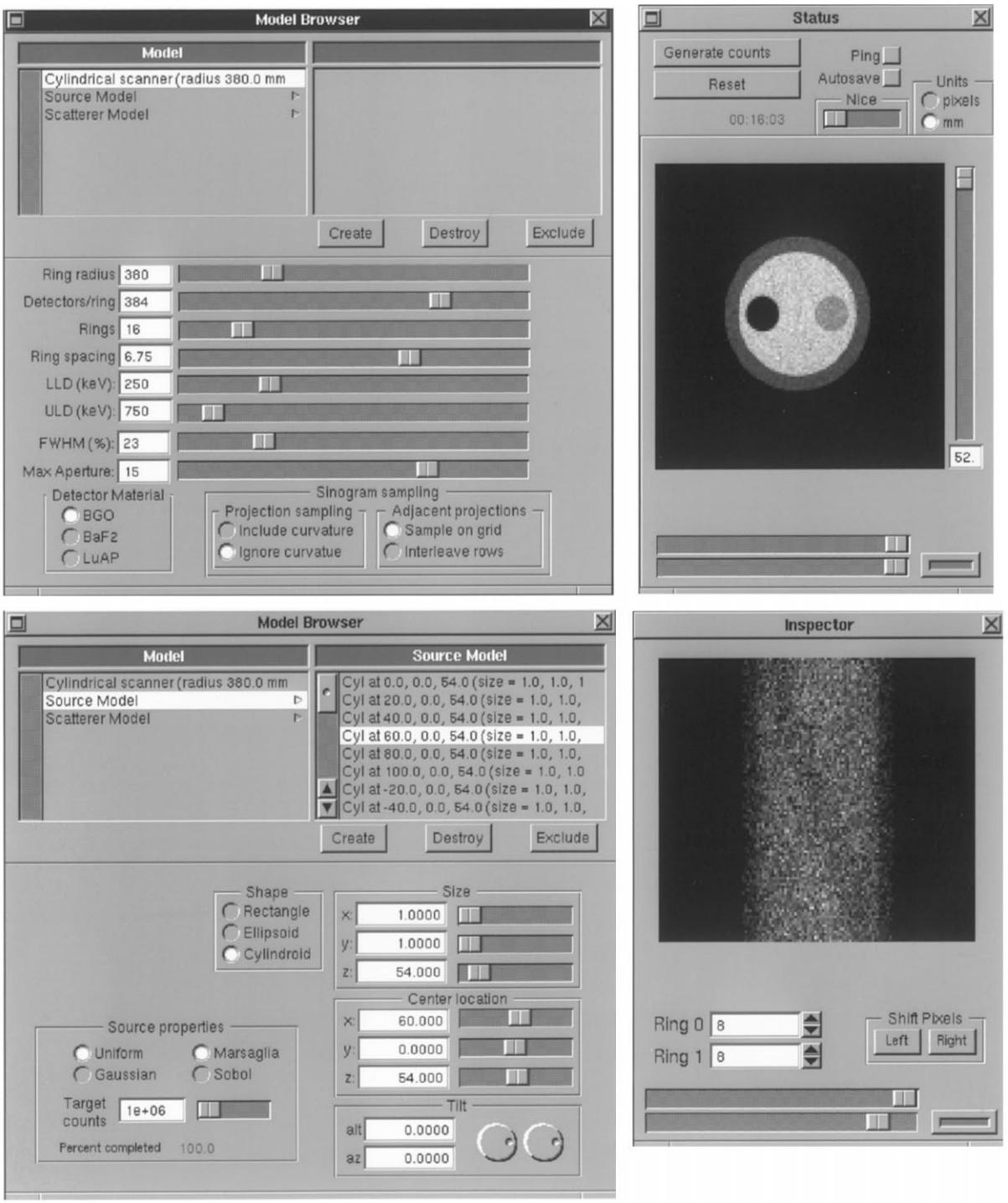

Fig. 3. User interface inspectors of the Monte Carlo simulator Eidolon describing scanner geometry (top left) and source distribution (bottom left). The reference image (top right) and the sinograms (bottom right) may be viewed as they are generated.

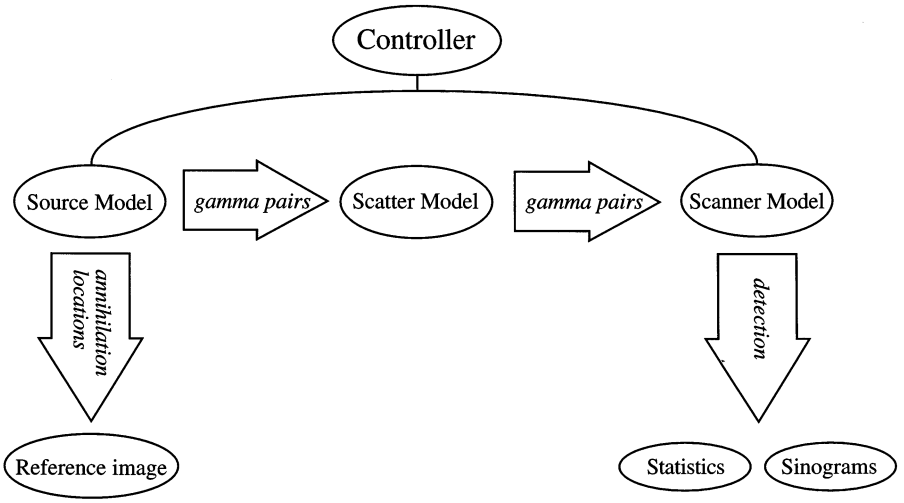

Fig. 4. A flow diagram showing the main components of the Monte Carlo simulator.

positron pair are not taken into account in the results presented here, but were included in the last version of the software.

Photoelectric absorption as well as incoherent and coherent scattering are taken into account to simulate photon interaction with scatter and detector objects. Interaction cross-sections and scattering distributions are computed from parametrizations implemented in the GEANT simulation package [24]. The total cross-section at the energy of the interacting photon determines the length of interaction. The relative ratios of the cross-sections for photoelectric effect to Compton (incoherent) and Rayleigh (coherent) scattering are used to choose randomly which process occurs at each interaction vertex. The distance x travelled by the photons before interacting is randomly generated according to the exponential distribution function $\mu e^{-\mu x}$, where μ represents the total linear attenuation coefficient. The Klein–Nishina angular distribution is used to sample the direction of the Compton scattered photons. The Marsaglia algorithm [25] was used to generate uniformly distributed pseudo-random numbers. This sequence of 24 bit pseudo-random numbers has a period of about 2^{144} and has passed stringent statistical tests for randomness and independence.

Interaction within scatter or detector objects can be switched on and off. In case interaction within detector objects is switched off, any photon impinging on a detector is assumed to deposit all its energy in the detector crystal. In the other case, photon pairs are recorded once two photons resulting from one annihilation event have passed the energy window set for discrimination. Random coincidences are not simulated. At each interaction vertex, the energy lost by the absorbed or scattered photon is assumed to be converted to scintillation light. Instead of tracking scintillation light in the detectors, energy resolution $\Delta E/E$ of the detector is simulated by convolving the deposited energy with a Gaussian function. $\Delta E/E$ is assumed to be proportional to $1/\sqrt{E}$.

3. Phantom simulations and computing time performances

Eidolon was used to simulate a uniform water-filled cylindrical phantom and the Utah phantom (Fig. 5) which was designed with a high degree of inhomogeneity both transaxially and axially in order to compare and test scatter correction techniques in 3D PET [26]. Phantom data sets were generated for the ECAT-953B PET scanner operated in 3D mode (16 rings of 384 detectors each

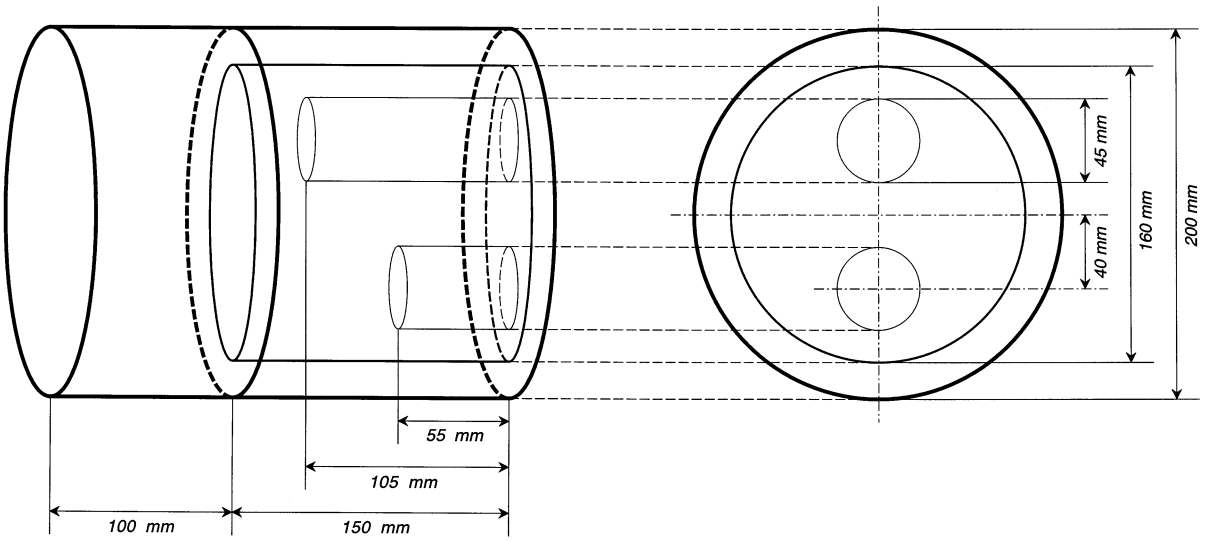

Fig. 5. Diagram of the Utah phantom.

with a ring radius of 38 cm) [27] both with and without scatter simulation. Detector energy resolution $\Delta E/E$ was set to 23% for 511 keV photons. The outer compartment of the Utah phantom, which is generally used to provide activity from outside the FOV, was left empty. Although studies of this effect could easily be performed with the program. Before reconstruction, attenuation correction was applied to those data sets generated with scatter simulation, attenuation correction files were created by forward projecting the 3D density map estimated with a constant linear attenuation coefficient of 0.096 cm^{-1}. No scatter correction was applied to the sets generated with scatter simulation. Generated data sets were reconstructed using four different 3D reconstruction algorithms implemented on a high-performance parallel platform [28].

In Fig. 6, projections of the central slice of a uniform phantom reconstructed before and after applying attenuation corrections to the data set generated with scatter simulation are shown. Fig. 7 shows transaxial slices of the Utah phantom reconstructed using the reprojection algorithm (PROMIS) [29], the fast volume reconstruction algorithm (FAVOR) [30], the Fourier rebinning algorithm (FORE) [31] and the single slice rebinning algorithm (SSRB) [32].

The time needed to perform a simulation study depends on the complexity of the chosen sets of source, scatter and detector objects and on selected interactions. The average time to track one coincident detection for the ECAT-953B PET scanner is 1.15 ms without scattering and attenuation. It increases to 11 ms if photon interactions are simulated within a single uniform scatter object corresponding to a 20 cm diameter cylinder filled with water and to 15.2 ms if they are simulated within both the scatter and detector objects.

4. Results

Eidolon was used to obtain unscattered and scattered energy distributions of coincident detections (Fig. 8), as well as to study line-spread functions (Fig. 9) and scatter fractions for the ECAT-953B PET scanner. In a real measurement, scatter components in the detectors and in the FOV are indistinguishable from other secondary effects. Monte Carlo simulation of energy distributions provide insight into the scattering processes arising in 3D positron tomography.

The scatter fraction is defined as the ratio between the number of coincident detections with at least one photon scattered in the FOV and the

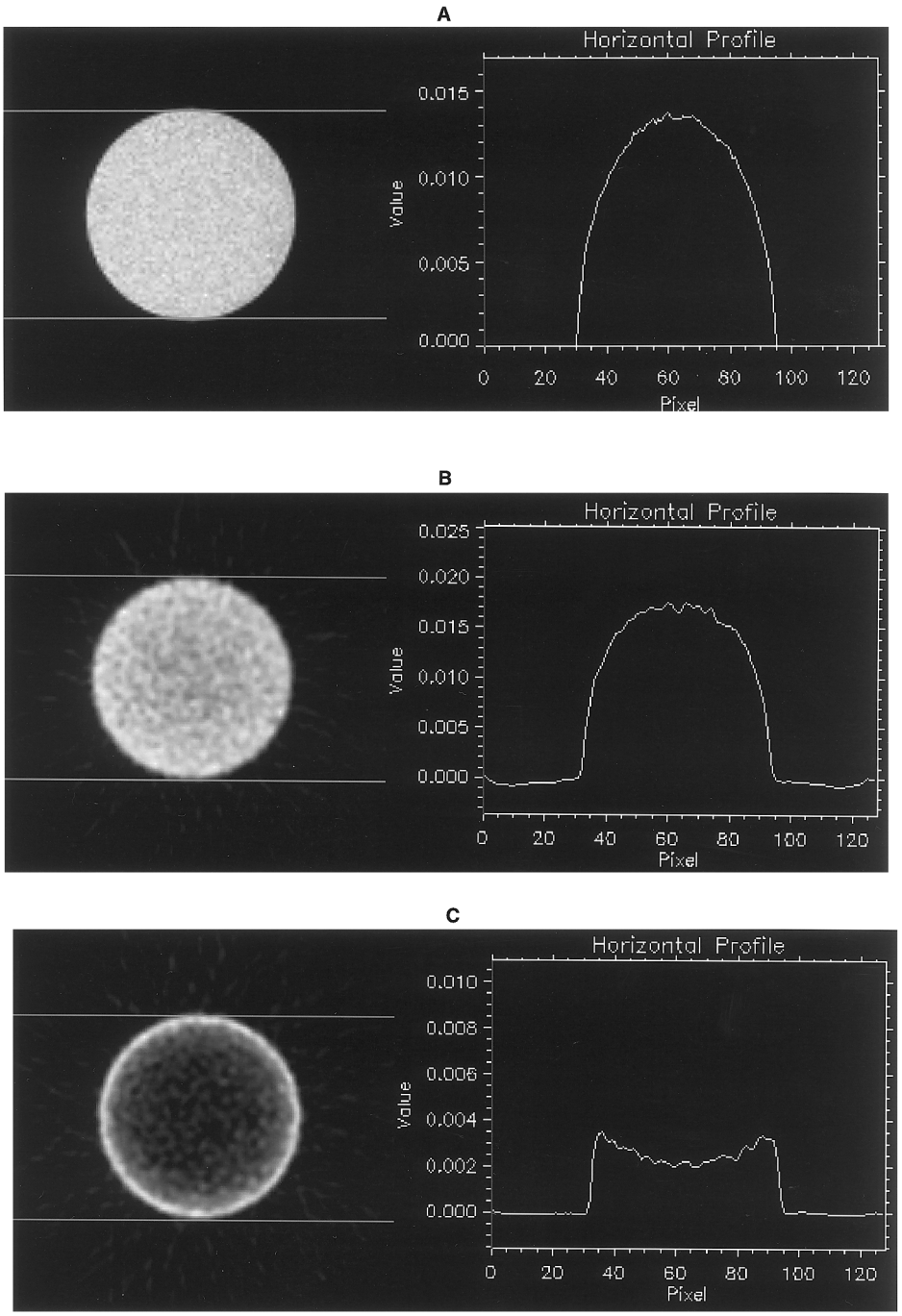

Fig. 6. Central slice and projections of a uniform cylindrical phantom. (A) Reference image. (B) Image reconstructed from a data set generated without scatter simulation. (C) Image reconstructed before attenuation corrections from a data set generated with scatter simulation. (D) Image reconstructed after applying attenuation corrections to the same data set as in C.

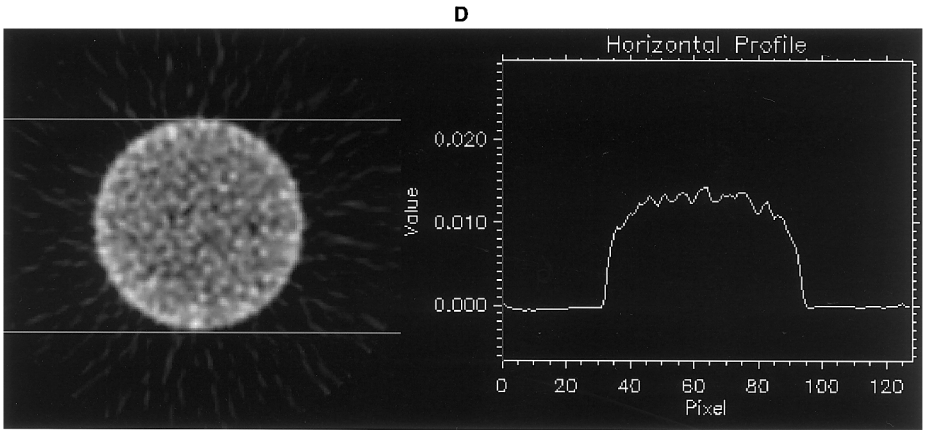

Fig. 6. (*Continued*)

total number of coincident detections. The scatter fraction was evaluated using the events' Monte Carlo history. Table 1 shows scatter fractions obtained with Eidolon for three different radial positions of a line source placed in a 20 cm diameter cylinder filled with water. Ten million annihilation events were generated for each radial position of the line source. To allow comparison with measurements, detector scatters were not counted, since they are usually not differentiated from the trues in experimental data. The scatter fraction determined with the line source in the centre of the phantom is 0.37. In the same detection conditions, a real measurement of this scatter fraction gave 0.42 [33], it was estimated to be 0.46 using a different Monte Carlo simulator [9]. The discrepancy between our value and the one given by Michel et al. [9] results from the fact that we did not consider those photons scattered only within the detector crystals as part of the scatter fraction. Consistent with the real measurements, our results show that the scatter fraction decreases when the source moves off-axis.

Our investigation of detector crosstalk shows that the proportion of detected photons depositing only part of their energy in the first crystal of interaction is significant and exceeds 50% which is in good agreement with the results reported in the literature [34]. Scatter fractions determined using simulation of the Utah phantom when varying the lower energy discrimination threshold are shown in Fig. 10. As the threshold is lowered, the scatter fraction increases steadily [33].

5. Discussion and conclusion

Although variance reduction techniques may be used to reduce computation time, the main drawback of the Monte Carlo method is that it is extremely time-consuming. Object-oriented programming also results in an undeniable computing time performance penalty associated with the service requests between the objects, because they are implemented as function calls. Moreover, objects are created and destroyed at a huge rate and the dynamic memory allocation/deallocation increases the execution time.

Nevertheless, the burden of computing time may be circumvent with the development of faster computers and parallel processing architectures. Furthermore, an Objective-C compiler is provided with the GNU C compiler available from the Free Software Foundation [35] and the current distributions of GNU CC (since version 2.7.1) include an Objective-C compiler and a runtime library. This makes possible to port Eidolon on most of the current platforms and operating systems. An implementation of Eidolon on a high-performance parallel platform consisting of 8 PowerPC-604 nodes recently installed in our laboratory is presently under evaluation [36].

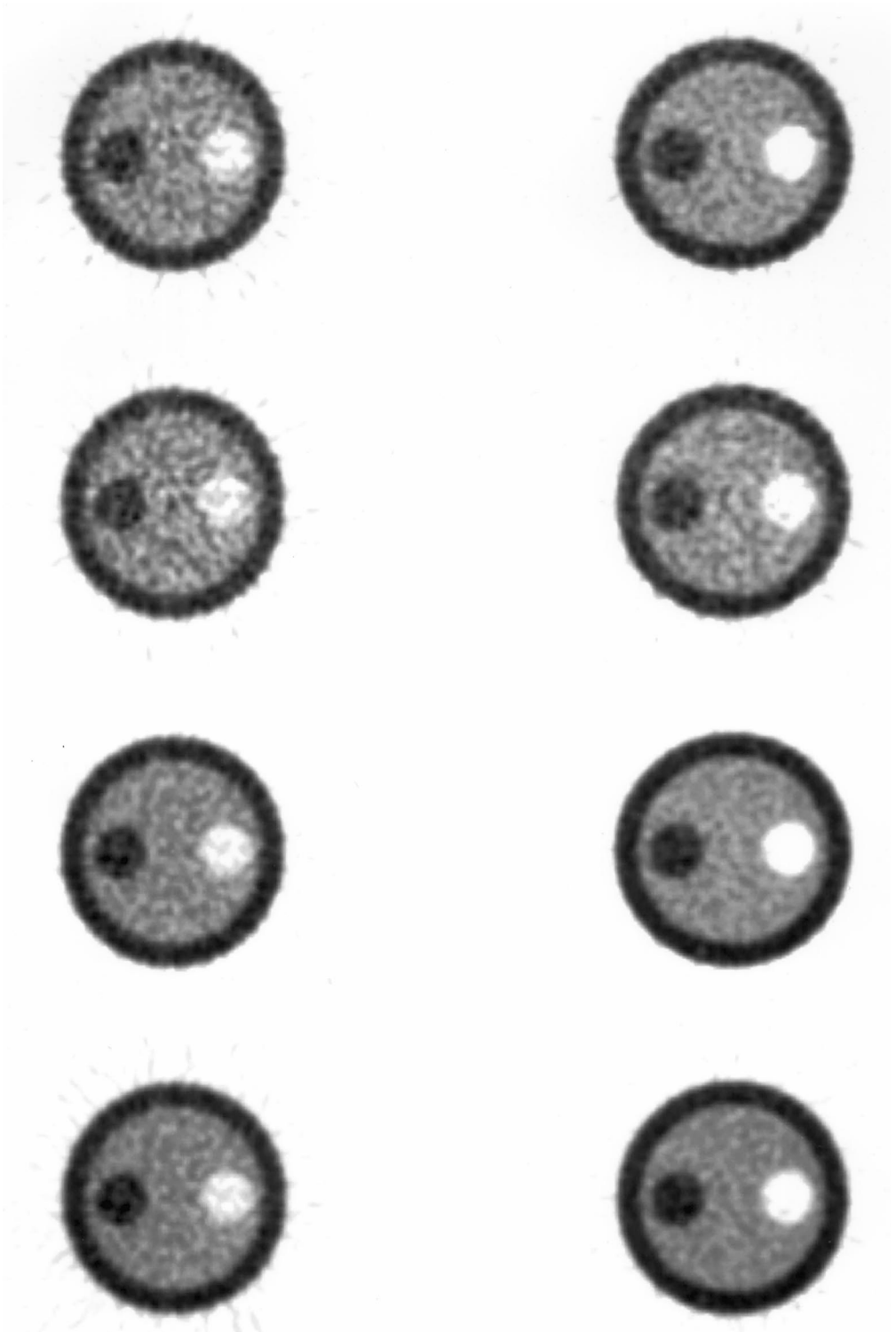

Fig. 7. Eleventh slice reconstructions of Monte Carlo data sets of the Utah phantom generated without (left) and with (right) scatter simulation using from top to bottom the PROMIS, FAVOR, FORE and SSRB algorithms. Approximately 16 million coincident detections were recorded for both types of simulation. The maximum obliquity used for reconstruction corresponds to a ring index difference of 11. No additional polar or azimuthal mashing was used. The image volume is a cylinder of radius 63 voxels by 31 transaxial slices. Normalised horizontal profiles through the centre of the slices are also shown.

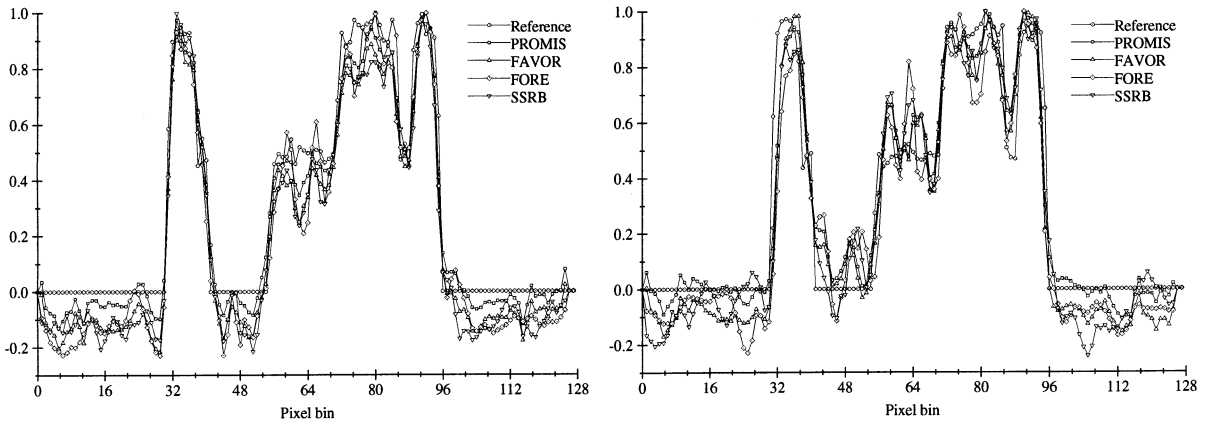

Fig. 7. *(Continued)*

Validation of image reconstruction implementations and scatter correction techniques using the Monte Carlo method have received considerable attention during the last decade. Monte Carlo modelling allows to separate the detected photons into their components: primary events, scatter events, contribution of down-scatter events, etc. and to perform detailed investigations of the spatial and energy distribution of Compton scatter which would be difficult to perform using present experimental techniques. Although several approaches have been proposed for scatter correction for 3D PET, five basic approaches have been taken to this correction: multi-energy window approaches, integral transformation approaches, an approach relying on an auxiliary, septa extended scan, curve-fitting approaches and model-based approaches. A comparative evaluation of the performance of different correction techniques is one of the interesting applications of the simulator.

The powerful constructs promoted by object technology can yield elegant, quality code. The object-oriented paradigm makes it possible to envision incremental refinements to any of the elements described in this paper with maximum code reuse by providing a framework for effectively defining standards using the inheritance mechanism. This approach streamlines development and

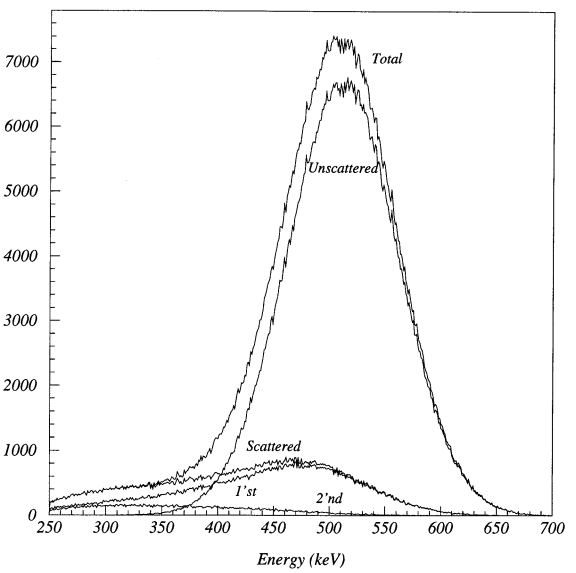

Fig. 8. Energy distributions of coincident detections resulting from the simulation of a line source placed in the centre of a 20 cm diameter cylinder filled with water. Photons impinging on a detector are assumed to deposit all their energy in the detector crystal. Energy resolution is proportional to the inverse square root of the deposited energy and is simulated by convolving the deposited energy with a Gaussian function whose FWHM is 23% for 511 keV photons. Both photons of a coincident detection have to pass an energy window set between 250 and 850 keV. Distributions of photons resulting from exactly one or two successive Compton scatterings in the field-of-view are shown.

Table 1
Comparison between Monte Carlo estimations and real measurements of the scatter fraction for different radial positions of a line source placed in a 20 cm diameter cylinder filled with water

Radial position (mm)	Eidolon	Spinks et al. [33]	Michel et al. [9]
0	0.37	0.42	0.46
40	0.36	0.40	
80	0.29	0.30	

Same detection conditions as in Fig. 8 apply, except that interaction within detector objects was switched on and energy window was set between 380 and 850 keV for comparison with published data.

improves reliability. It makes Eidolon a very powerful tool that can be further improved to evaluate new possible designs for future high-performance positron tomographs. Eventually, Eidolon will be exploited to explore different strategies of sampling schemes of the 3D X-ray transform and possibly as a forward projector that includes accurate attenuation and scatter modelling for iterative reconstruction algorithms.

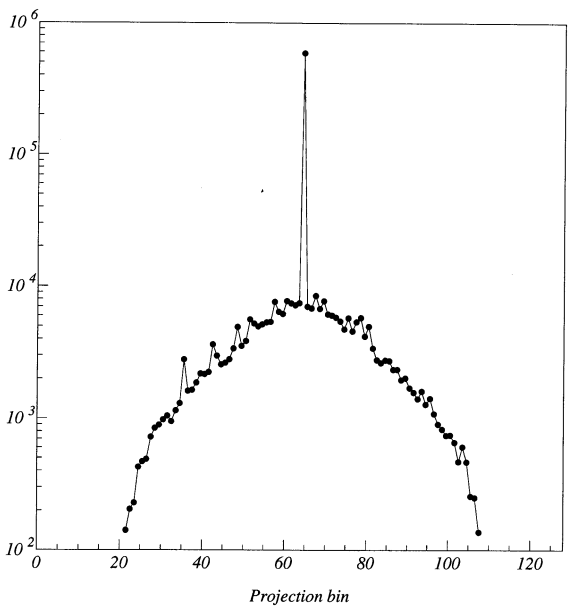

Fig. 9. Sum of one-dimensional transaxial projections resulting from the simulation of a line source placed in a 20 cm diameter cylinder filled with water. Same detection conditions as in Fig. 8 apply.

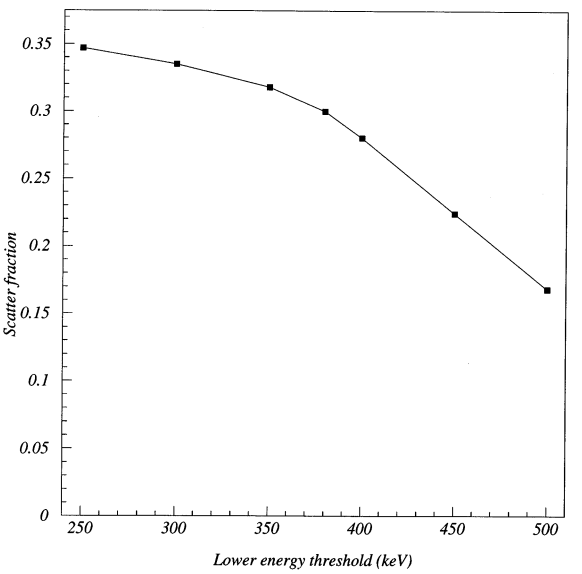

Fig. 10. Variation of scatter fraction determined for the Utah phantom as a function of the lower energy discrimination threshold.

6. Program availability

The program running under the NextStep environment as described in this paper is freely available from the authors.

Acknowledgements

This work was supported in part by the Schmidheiny Foundation, the Swiss Federal

Office for Education and Science under grant E3260 within the European Esprit project HARMONY (CE 7253) and the Swiss National Science Foundation under project 2100-043627.95.

References

[1] P. Andreo, Monte Carlo techniques in medical radiation physics, Phys. Med. Biol. 36 (1991) 861–920.
[2] M. Tagesson, M. Ljungberg, S.-E. Strand, A Monte Carlo program converting activity distributions to absorbed dose distributions in a radionuclide treatment planning system, Acta Oncol. 35 (1996) 367–372.
[3] M. Ljungberg, S.-E. Strand, A Monte Carlo program for the simulation of scintillation camera characteristics, Comput. Methods Programs Biomed. 29 (1989) 257–272.
[4] G. Tsang, C. Moisan, J.G. Rogers, A simulation to model position encoding multicrystal PET detectors, IEEE Trans. Nucl. Sci. 42 (1995) 2236–2243.
[5] S. Delorme, R. Frei, C. Jospeh, J.-F. Loude, C. Morel, Use of a neural network to exploit light division in a triangular scintillating crystal, Nucl. Instrum. Method A 373 (1996) 111–118.
[6] K.A. Comanor, P.R.G. Virador, W.W. Moses, Algorithms to identify detector Compton scatter in PET modules, IEEE Trans. Nucl. Sci. 43 (1996) 2213–2218.
[7] D. Vozza, C. Moisan, S. Paquet, An improved model for energy resolution of multicrystal encoding detectors for PET, IEEE Trans. Nucl. Sci. 44 (1997) 179–183.
[8] D. Bollini, A. Del Guerra, G. Di Domenico, M. Galli, M. Gambaccini, G. Zavattini, Sub-millimeter planar imaging with positron emitters: EGS4 code simulation and experimental results, IEEE Trans. Nucl. Sci. 44 (1997) 1499–1502.
[9] C. Michel, A. Bol, T. Spinks, D.W. Townsend, D. Bailey, S. Grootoonk, T. Jones, Assessment of response function in two PET scanners with and without interplane septa, IEEE Trans. Med. Imag. 10 (1991) 240–248.
[10] C.J. Thompson, J-M. Cantu, Y. Picard, PETSIM: Monte Carlo program simulation of all sensitivity and resolution parameters of cylindrical positron imaging systems, Phys. Med. Biol. 37 (1992) 731–749.
[11] R.L. Harrison, S.D. Vannoy, D.R. Haynor, S.B. Gillispie, M.S. Kaplan, T.K. Lewellen, Preliminary experience with the photon history generator module for a public-domain simulation system for emission tomography, in: Conf. Rec. IEEE Med. Imag. Conf., San Francisco, 1993, pp. 1154–1158 (New York IEEE, 1994).
[12] M.I. Lopes, V. Chepel, J.C. Carvalho, R. Ferreira Marques, A.J.P.L. Policarpo, Performance analysis based on a Monte Carlo simulation of a liquid Xenon PET detector, IEEE Trans. Nucl. Sci. 42 (1995) 2298–2302.
[13] R.R. Raylman, B.E. Hammer, N.L. Christensen, Combined MRI-PET scanner: a Monte Carlo evaluation of the improvements in PET resolution due to the effects of a static homogeneous magnetic field, IEEE Trans. Nucl. Sci. 43 (1996) 2406–2412.
[14] S. Pavlopoulos, G. Tzanakos, Design and performance evaluation of a high-resolution small animal positron tomograph, IEEE Trans. Nucl. Sci. 43 (1996) 3249–3255.
[15] W.W. Moses, P.R.G. Virador, S.E. Derenzo, R.H. Huesman, T.F. Budinger, Design of a high-resolution, high-sensitivity PET camera for human brains and small animals, IEEE Trans. Nucl. Sci. 44 (1997) 1487–1491.
[16] D.W. Litzenberg, F.D. Becchetti, D.A. Roberts, On-line PET monitoring of radiotherapy beams: image reconstruction and Monte Carlo simulations of detector geometries, IEEE Trans. Nucl. Sci. 44 (1997) 1646–1657.
[17] A.K. Herrmann Scheurer, M.L. Egger, C. Joseph, C. Morel, A Monte Carlo phantom simulator for positron emission tomoraphy, in: H.J. Hermann, D.E. Wolf, E. Pöppel (Eds.), Proceedings of the Workshop on Supercomputing in brain research: from tomography to neural networks, Jülich, 1994, pp. 205–209 (World Scientific Publishing, 1995).
[18] H. Zaidi, A. Herrmann Scheurer, C. Morel, Development of an object-oriented Monte Carlo simulator for 3D positron tomography, in: P. Kinahan, D. Townsend (Eds.), Conf. Rec. of the International Meeting in Fully Three-Dimensional Image Reconstruction in Radiology and Nuclear Medicine, Nemacolin Woodlands, 1997, pp. 176–179, (UPMC, Pittsburgh, PA, 1997).
[19] C.C. Watson, D. Newport, M.E. Casey, A. deKemp, R.S. Beanlands, M. Schmand, Evaluation of simulation-based scatter correction for 3-D PET cardiac imaging, IEEE Trans. Nucl. Sci. 44 (1997) 90–97.
[20] D.R. Haynor, R.L. Harrison, T.K. Lewellen, Energy-based scatter correction for 3D PET: a Monte Carlo study of best possible results, in: P. Kinahan; D. Townsend (Eds.), Conf. Rec. of the International Meeting in Fully Three-Dimensional Image Reconstruction in Radiology and Nuclear Medicine, Nemacolin Woodlands, 1997, pp. 52–54, (UPMC, Pittsburgh, PA, 1997).
[21] L. Desbat, Efficient sampling in 3D tomography, in: P. Grangeat (Eds.), Conf. Rec. of the International Meeting in Fully Three-Dimensional Image Reconstruction in Radiology and Nuclear Medicine, Aix-les-Bains, 1995, pp. 281–285, (LETI, Grenoble, 1995).
[22] NEXSTEP object-oriented programming and the objective C language (NeXT Computer, Redwood City, CA, 1992).
[23] NEXSTEP development tools and techniques (NeXT Computer, Redwood City, CA, 1992).
[24] R. Brun, F. Bruyant, M. Maire, A.C. McPherson, P. Zanarini, GEANT 3 (CERN DD/EE/84-1, 1987).
[25] G. Marsaglia, A. Zaman, Monkey tests for random number generators, Comp. Math. Appl. 23 (1993) 1–10.
[26] D.W. Townsend, Y. Choi, D. Sashin, M.A. Mintun, An investigation of practical scatter correction techniques for 3D PET, J. Nucl. Med. 35 (1994) 50 Abstract.

[27] B. Mazoyer, R. Trebossen, R. Deutsch, M. Casey, K. Blohm, Physical characteristics of the ECAT 953B/31: a new high resolution brain positron tomograph, IEEE Trans. Med. Imag. 10 (1991) 499–504.
[28] M.L. Egger, A.K. Herrman Scheurer, C. Joseph, C. Morel, Fast volume reconstruction in positron emission tomography: implementation of four algorithms on a high-performance scalable parallel platform, in: Conf. Rec. IEEE Med. Imag. Conf., Anaheim, CA, 1996, pp. 1574–1578 (New York IEEE, 1997).
[29] P.E. Kinahan, J.G. Rogers, Analytic 3D image reconstruction using all detected events, IEEE Trans. Nucl. Sci. 36 (1989) 964–968.
[30] M. Defrise, D.W. Townsend, R. Clack, FAVOR: a fast reconstruction algorithm for volume imaging in PET, in: Conf. Rec. 1991 IEEE Medical Imag. Conf., Santa Fe, 1991, pp. 1919–1923 (New York IEEE, 1992).
[31] M. Defrise, A factorization method for the 3D X-ray transform, Inverse Prob. 11 (1995) 983–994.
[32] M.E. Daube-Witherspoon, G. Muehllehner, Treatment of axial data in three-dimensional PET, J. Nucl. Med. 82 (1987) 1717–1724.
[33] T.J. Spinks, T. Jones, D.L. Bailey, D.W. Townsend, S. Grootoonk, P.M. Bloomfield, M.-C. Gilardi, M.E. Casey, B. Sipe, J. Reed, Physical performance of a positron tomograph for brain imaging with retractable septa, Phys. Med. Biol. 37 (1992) 1637–1655.
[34] M. Bentourkia, P. Msaki, J. Cadorette, R. Lecomte, Object and detector scatter function dependence on energy and position in high resolution PET, IEEE Trans. Nucl. Sci. 42 (1995) 1162–1167.
[35] Free Software Foundation, Boston, MA 02111-1307 USA.
[36] H. Zaidi, C. Labbé, C. Morel, Implementation of a Monte Carlo simulation environment for fully 3D PET on a high-performance parallel platform, Parallel Computing 10 (1998) 1523–1536.